A GLOBAL 3D P-VELOCITY MODEL OF THE EARTH'S CRUST AND MANTLE FOR IMPROVED EVENT LOCATION -- SALSA3D

Sanford Ballard[1], Michael A. Begnaud[2], Christopher J. Young[1], James R. Hipp[1], Marcus Chang[1], Andre V. Encarnacao[1], Charlotte A. Rowe[2], W. Scott Phillips[2], and Lee K. Steck[2]

[1]Sandia National Laboratories and [2]Los Alamos National Laboratory

Sponsored by the National Nuclear Security Administration

Award Nos. DE-AC04-94AL8500/SL09-3D Earth-NDD02[1], and DE-AC52-06NA25396/LA09-IRP-NDD02[2]

ABSTRACT

To test the hypothesis that high quality 3D Earth models will produce seismic event locations which are more accurate and more precise, we are developing a global 3D P wave velocity model of the Earth's crust and mantle using seismic tomography. In this paper, we present the most recent version of our model, SALSA3D (SAndia LoS Alamos) version 1.4, and demonstrate its ability to reduce mislocations for a large set of realizations derived from a carefully chosen set of globally-distributed ground truth events.

Our model is derived from the latest version of the Ground Truth (GT) catalog of P and Pn travel time picks assembled by Los Alamos National Laboratory. To prevent over-weighting due to ray path redundancy and to reduce the computational burden, we cluster rays to produce representative rays. Reduction in the total number of ray paths is > 55%. The model is represented using the triangular tessellation system described by Ballard et al. (2009), which incorporates variable resolution in both the geographic and radial dimensions. For our starting model, we use a simplified two layer crustal model derived from the Crust 2.0 model over a uniform AK135 mantle. Sufficient damping is used to reduce velocity adjustments so that ray path changes between iterations are small. We obtain proper model smoothness by using progressive grid refinement, refining the grid only around areas with significant velocity changes from the starting model. At each grid refinement level except the last one we limit the number of iterations to prevent convergence thereby preserving aspects of broad features resolved at coarser resolutions. Our approach produces a smooth, multi-resolution model with node density appropriate to both ray coverage and the velocity gradients required by the data. This scheme is computationally expensive, so we use a distributed computing framework based on the Java Parallel Processing Framework, providing us with ~400 processors. Resolution of our model is assessed using a variation of the standard checkerboard method, as well as by directly estimating the diagonal of the model resolution matrix based on the technique developed by Bekas, et al.

We compare the travel-time prediction and location capabilities of this model over standard 1D models. We perform location tests on a global, geographically-distributed event set with ground truth levels of 5 km or better. These events generally possess hundreds of Pn and P phases from which we can generate different realizations of station distributions, yielding a range of azimuthal coverage and proportions of teleseismic to regional arrivals, with which we test the robustness and quality of relocation. The SALSA3D model reduces mislocation over standard 1D ak135, especially with increasing azimuthal gap. The 3D model appears to perform better for locations based solely or dominantly on regional arrivals, which is not unexpected given that ak135 represents a global average and cannot therefore capture local and regional variations.

INTRODUCTION

The evolving U.S. monitoring needs require accurate location of smaller and smaller events. Given the limited station coverage of a typical global monitoring network, such as the International Monitoring System (IMS), it is likely that such events will be detected by a small number of stations, quite possibly with a poor network geometry. For locating such events, it is essential to have extremely high fidelity travel time predictions, particularly at regional distances where lateral heterogeneity can be significant. Accurately accounting for lateral heterogeneity implies using 3D models of the Earth to calculate travel times, but relatively few of the available 3D Earth models are appropriate for high fidelity travel time prediction, and it is unclear whether any of those that are appropriate actually improve event locations. Thus, we are developing our own global 3D P wave velocity model of the Earth's crust and mantle -- SALSA3D (SAndia LoS Alamos 3D) -- using seismic tomography based on a carefully assembled data set of P phase travel times collected by LANL over the past decade. An important difference between our effort and previous efforts is that our model was produced specifically for improving event location; the model provides potentially valuable information about the structure of the Earth, but this is not our focus. Hence, all decisions about data processing and tomography were made with this goal in mind.

In this paper, we present the most recent version of our model, SALSA3D version 1.4, and demonstrate its ability to reduce mislocations for a large set of realizations derived from a carefully chosen set of globally-distributed ground truth events.

DATA SET

The data used for the tomographic inversion was collected by LANL over the past decade and includes events categorized with a ground truth (GT) level of 25 km or better (Bondár et al., 2004). Arrivals for these GT events were merged from various sources in order to produce a single set of arrivals for each event with redundancies removed, maximizing the available arrivals for each event (Begnaud, 2005). Regional Pn and teleseismic P arrivals were extracted for use in the tomography and resulted in ~119K events, ~12K stations, and almost 12 million individual ray paths (Figure 1). Geographically focused component data sets include USarray and the Deep Seismic Soundings in the former Soviet Union (e.g., Li and Mooney, 1998). To prevent over-weighting due to ray path redundancy and to reduce the computational burden, we cluster rays to produce representative rays, thereby reducing the total number of ray paths by 55%.

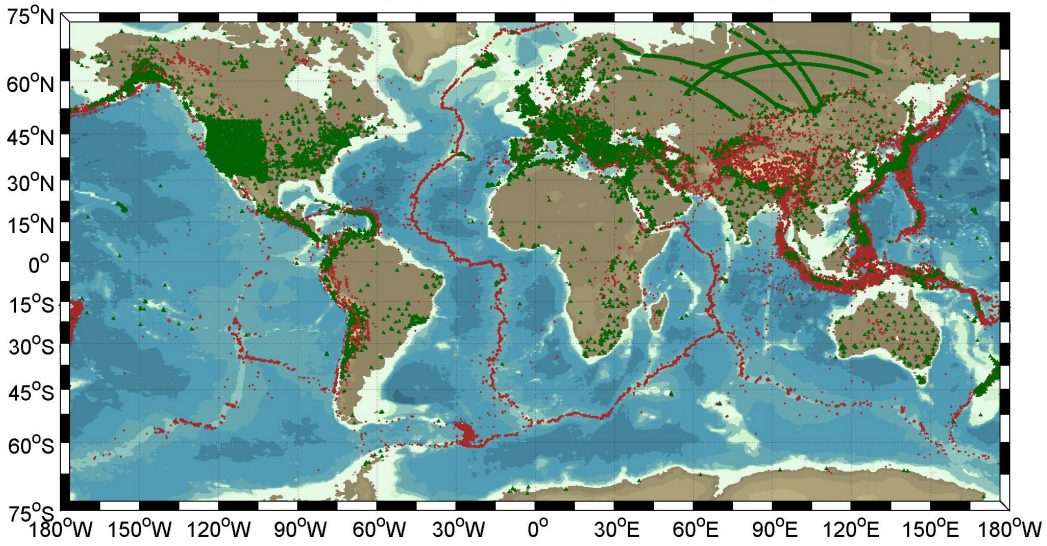

Figure 1. Stations and events used for the global tomography inversion. These data were collected by LANL over the past decade and are all categorized with a ground truth level of 25 km or better.

TOMOGRAPHIC INVERSION

We use the LSQR algorithm of Paige and Saunders (1982) to invert the data to find the P wave velocity distribution in the mantle that optimally reduces the misfit between observed and predicted travel times for P and Pn phase arrivals. Our starting model for the inversion consists of a modified version of the Crust 2.0 model (Laske and Masters, 1997, Laske et al., http://igppweb.ucsd.edu/~gabi/crust2.html) overlaying an AK135 mantle. We modify Crust 2.0 by combining their six layers into just two. The crust is damped heavily in the inversion so it changes very little. We retrace the rays at each of 16 iterations using the pseudo-bending algorithm (Um and Thurber, 1987, Zhao and Lei, 2004, Ballard et al., 2009). During early iterations, the mantle is moderately damped to discourage the inversion from progressing too rapidly but then damping is relaxed in later iterations. Adding regularization constraints to the data kernal matrix is not required during the inversion since it is accomplished by beginning with a coarse grid that is progressively refined several times during the inversion (Simmons et al., 2009).

ADAPTIVE GRID REFINEMENT

P wave velocity in our model is stored on a 3D grid of nodes that has variable resolution in both geographic and radial dimensions. Our basic starting point is a 2 dimensional, multi-level triangular tessellation of a unit sphere (Wang and Dahlen, 1995, Ballard et al., 2009). We assign a tessellation with 8° triangles to the lower mantle, a tessellation with 4° triangles to the transition zone and upper mantle, and a third tessellation with variable resolution to all crustal layers. The crustal tessellation (not shown) has 2° triangles in oceanic regions, 1° triangles in most continental regions, and 0.5° triangles in the United States where the additional resolution is warranted due to the dense station coverage afforded by the USArray. The two tessellations in the mantle are refined, in both the geographical and radial dimensions, during the progress of the tomographic inversion. Figure 2 illustrates the final geographic node configuration of the tessellation assigned to the transition zone and upper mantle. 4° triangles in relatively aseismic parts of the world remain unrefined in the final, model, but the grid is refined down to triangles as small as 0.5° in areas with dense seismicity or stations, or both.

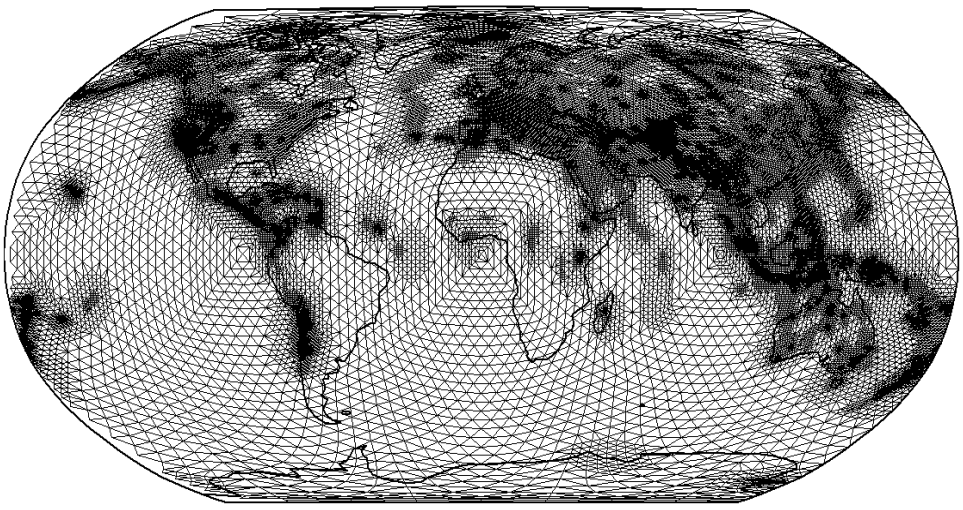

Figure 2. The final grid for the transition zone and upper mantle with triangle sizes ranging from 0.5° to 4°. The grid for these layers in the starting model consisted entirely of 4° triangles.

VELOCITY MODEL

A small portion of the global range of our model is illustrated in Figure 3 and Figure 4. The images reveal many tectonic features of the Earth. Major cratons in Siberia, North America, Southern Africa and Australia are all characterized by P wave velocities that are relatively fast compared to AK135. Tectonically active areas such as western North America and the Mediterranean region are relatively slow, as are the mid-ocean ridges in the Pacific, Atlantic and Indian Oceans. In subduction zones beneath the Andes, Sumatra and New Zealand we see fast oceanic slabs being subducted beneath the adjacent continents. The stagnant subducted slab beneath Japan is particularly evident in Figure 4. Very fast material is evident in the upper mantle beneath Tibet and slow velocity anomalies appear in the Red Sea region.

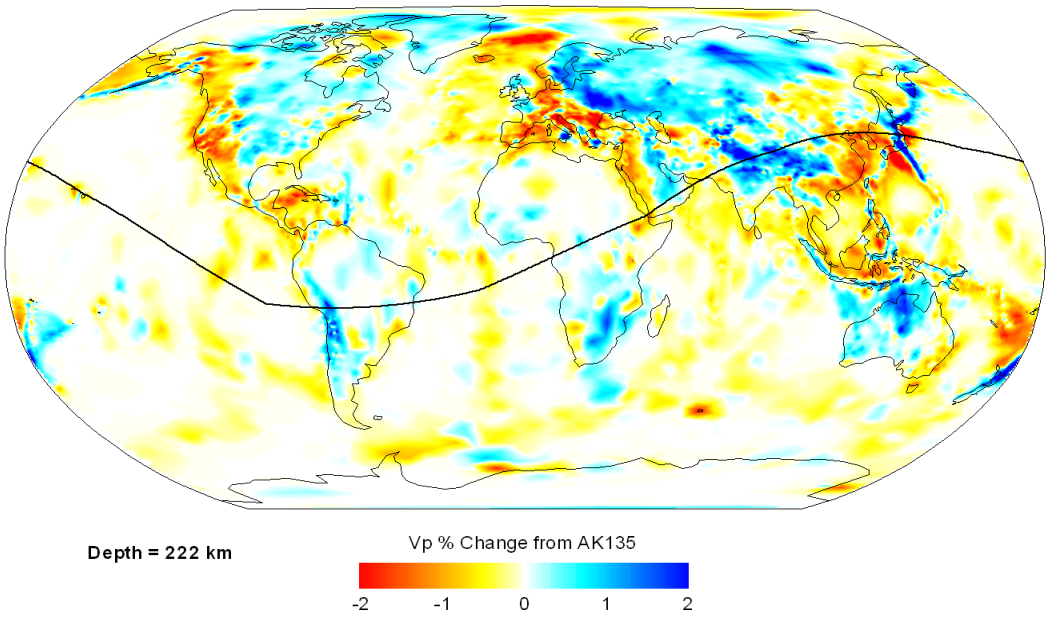

Figure 3. Map of the % difference in P wave velocity between SALSA3D and AK135 at a depth of 225 km in the upper mantle. The black line shows the position of the approximate great circle path of the cross section shown in Figure 4.

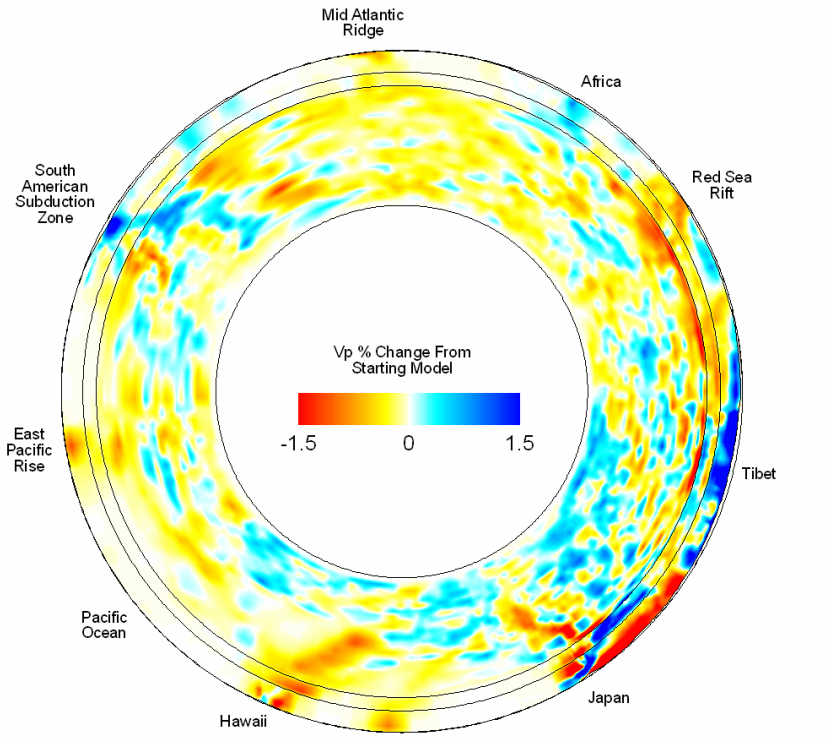

Figure 4. Cross section through SALSA3D at the location shown by the black line in Figure 3.

RESOLUTION TESTS

Images of tomographic models can provide important insight into fundamental questions about the structure of the Earth, such as the fate of subducting slabs. However, when interpreting these images, one must consider the

resolution of the tomographic inversion. For large models like ours, this can be a computationally challenging problem. A standard way to estimate model uncertainty is to create known detailed velocity structures (often "checkerboard" patterns), use these to create synthetic observations for the actual data paths, and then to invert these synthetic observations to see how much of the known structure can be recovered. This technique measures the theoretical resolution possible given the ray coverage (i.e. it is based entirely on ray geometries). The actual resolution is something less than this because the observations themselves will have errors.

We adopt the checkerboard technique here, though our pattern is slightly different, consisting of equal sized alternating velocity triangles, so that we can maintain the same feature size regardless of latitude (the rectangular latitude/longitude checkers used by many researchers actually get smaller towards the poles). Our checkers represent deviations relative to our final tomographic model so that the ray paths will be as realistic as possible. For the same reason, our checkers have relatively small deviations (+/- 1%) relative to the background model.

As expected given the ray coverage (Figure 1), our model resolution varies strongly both laterally and with depth. Resolution is best for Asia, due to the excellent coverage provided by the LANL GT data set. Resolution is best in the upper portion of the lower mantle, due to the large number of teleseismic raypaths in our dataset that bottom near this depth.

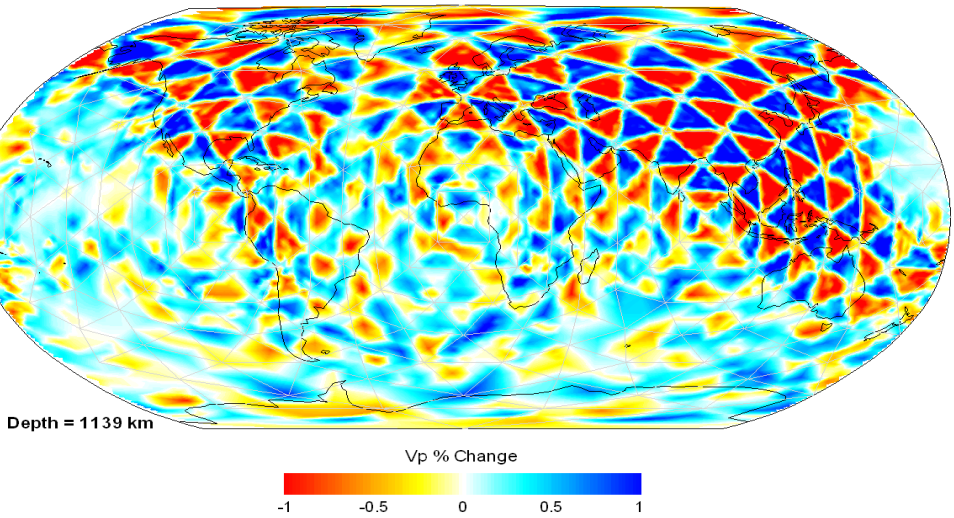

Figure 5. Results of the Chinese checkerboard test at a depth of 1139 km in the shallow part of the lower mantle.

TRAVEL TIME RESIDUAL REDUCTION

To evaluate the ability of our model to accurately predict observed source-receiver seismic travel times, we define a set of 19 polygons that surround areas of contiguous seismicity around the world (Figure 6). For each of the 49 seismic stations in the IMS primary network we compute the mean absolute residual (absolute value of observed minus predicted travel time) for all of the events in each polygon using the AK135 model (Kennett et al., 1995) and using SALSA3D. For computing the AK135 travel times we used the Taup Toolkit software package (Crotwell et al., 1999). The results, illustrated in Figure 7, indicate that SALSA3D produces travel time residuals that are smaller than those produced by AK135 more that 92% of the time.

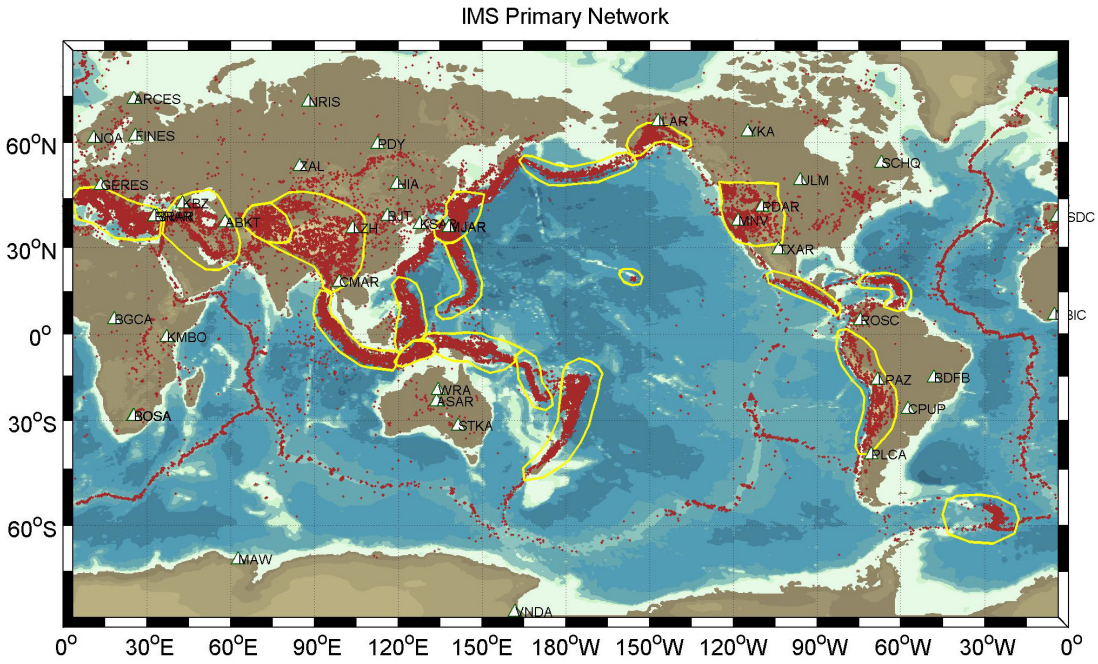

Figure 6. Map of the locations of the 49 IMS primary network stations and the 19 seismic regions selected for travel time residual analysis.

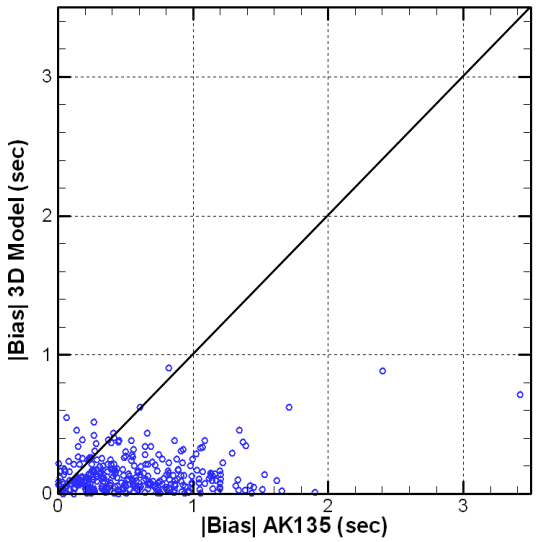

Figure 7. Median absolute value of residual computed with AK135 vs the same value computed with SALSA3D. Each point represents a single station-region pair.

LOCATION IMPROVEMENT

To test the location accuracy of the SALSA3D model, we selected a set of GT5 or better events from throughout Eurasia that contained enough Pn and P arrivals to be able to create a set of random realizations of differing station coverages. 42 events in Eurasia were initially selected and modified from the location test set of Myers et al. (2010), pulling data from the LANL GT database (Figure 8).

For each event, 5 random selections of P and Pn arrivals were made for each target number of arrivals from 5 to 50 (incremented by 1). The total number of realizations was 9585 (one event did not have 50 available phases).

Our event clustering process performed prior to the tomography significantly reduces any circularity issues despite the lack of a formal event segregation procedure.

We relocated each realization with the standard 1D AK135 model (Kennett et al, 1995) and our global SALSA3D tomography model. For AK135, we used the appropriate ellipticity/station corrections and the default model error. For SALSA3D, an estimated model error was used based on a summary standard deviation of residuals with distance. Results were evaluated based on median mislocations with the total number of phases, azimuthal gap, and the relative number of teleseismic P versus regional Pn.

Figure 9 shows the median mislocation of the relocated random realizations with azimuthal gap. At small azimuthal gaps, the median mislocation for the 3D model is slightly reduced over AK135, but the good station coverage produces accurate locations for either model. As the azimuthal gap increases, the use of the 3D model results in a greater reduction in mislocation over the 1D AK135 model by as much as a ~10 km.

Figure 10 shows the median mislocation using different combinations of P and Pn arrivals. The maximum number of any arrival set is 50. The SALSA3D model has an overall lower median mislocation. The combination of equal numbers of Pn and P arrivals results in the highest median mislocation values for the 1D AK135 model. This demonstrates the problems combining regional and teleseismic arrivals when using a model not designed for such a purpose. The results using the 3D model do not show this higher median mislocation in the area of equal P and Pn, indicating reduced problems with combining regional and teleseismic phases. Notice that results with fewer phases (< 10) clearly demonstrate improvement by the 3D model, as expected.

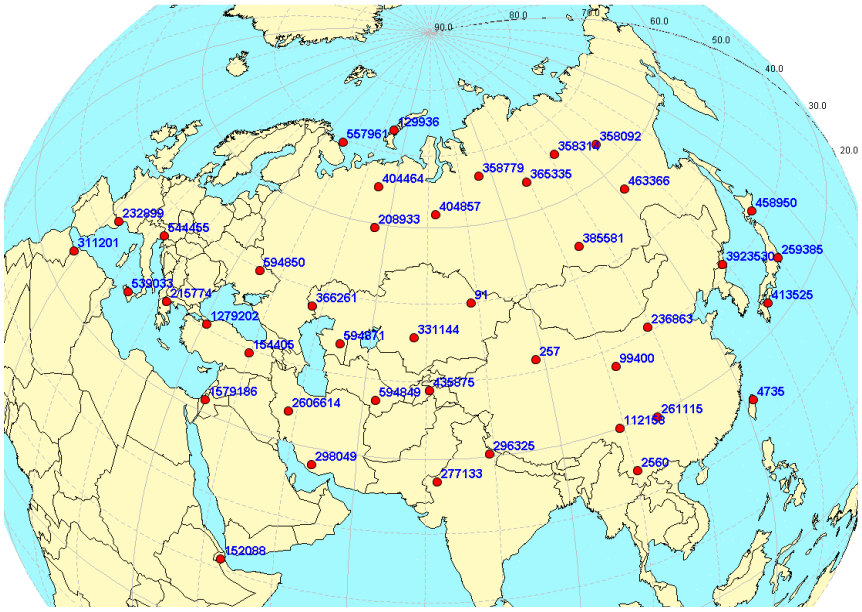

Figure 8. Validation events for location testing. 42 GT5 or better events were selected within Eurasia in order to produce a random data set of varying station/data configurations in which to test the location accuracy of the 3D model. The events were selected from Myers et al. (2010) with a few additional to improve spatial coverage.

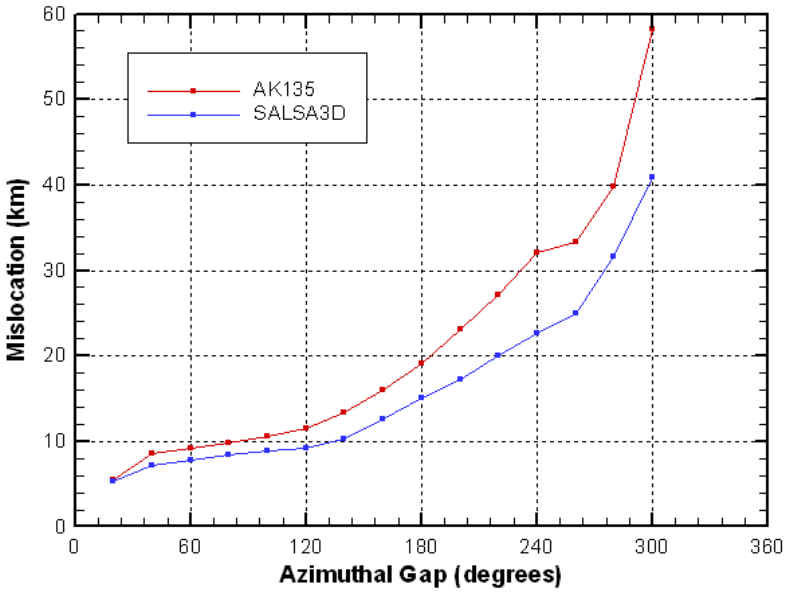

Figure 9. Median mislocation versus azimuthal gap for the location improvement testing using the random realizations of the 42 events shown in Figure 8.

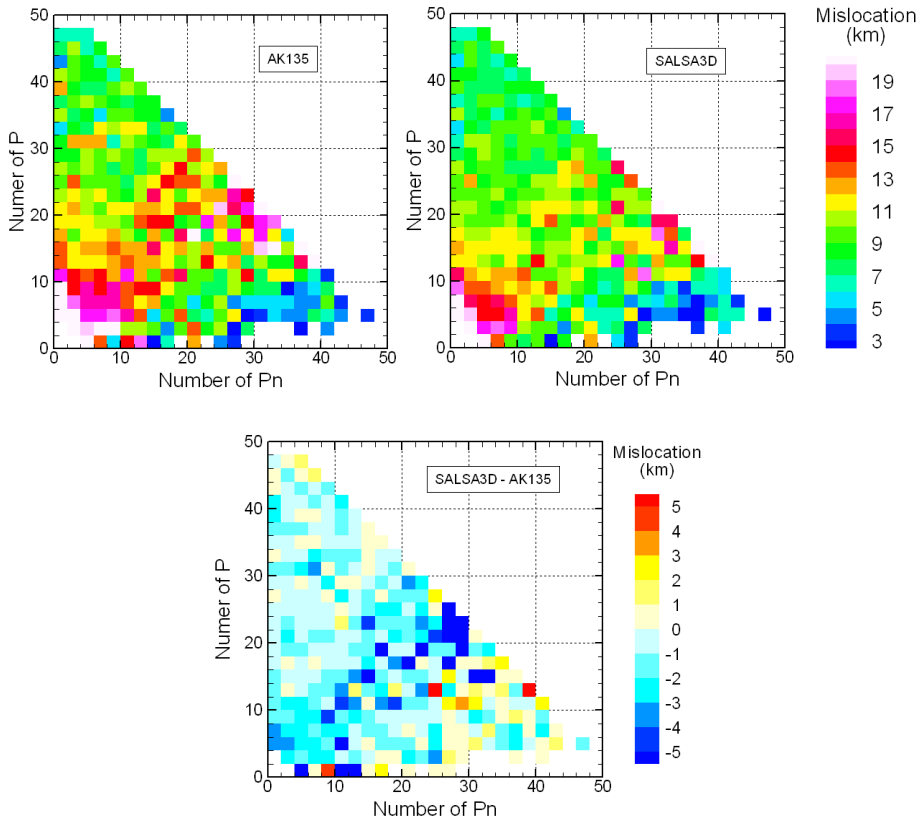

Figure 10. Median mislocation with varying number of P and Pn arrivals for the random realization location tests (bin size =2). The AK135 model results (top left) display higher mislocation values than the SALSA3D model (top right). The higher mislocation values at approximately equal numbers of P and Pn arrivals seen in the AK135 results are not observed for the 3D model. The mislocation difference between the models (bottom) shows that the 3D model is performing significantly better than AK135 for the majority of phase combinations.

CONCLUSION

In this paper, we have presented the latest version of SALSA3D, the Sandia-Los Alamos global tomography 3D P-velocity model of the crust and mantle. Our model is multi-resolution, with the resolution determined dynamically as part of the tomographic inversion. Additional nodes are added where ray coverage is high and velocity gradients are significant; other areas maintain the starting grid sampling. SALSA3D images many well-established features within the Earth, such as subducting slabs and continental roots, and is generally consistent with other recent global and regional models. Resolution, as established by checkerboard tests, is highly variable both laterally and with depth, with the best resolution in Asia and Europe in the upper part of the lower mantle.

More important than the structural features in the model is the fact that SALSA3D provides compelling improvement in travel time prediction and in event location compared to AK135. Evaluating performance for the IMS primary network, travel time residuals grouped by station and geographic region show clear improvements for virtually all combinations spanning a variety of distances and tectonic regions. Event location improvement is evaluated by re-locating multiple realizations from a set of 42 well-characterized events in Europe and Asia. SALSA3D improves locations only slightly when the number of stations is large, but as the number of phases drops, the 3D model does significantly better. Further, because our model is developed to fit both P and Pn data, it performs well with regional data, teleseismic data, or a combination of the two.

REFERENCES

Ballard, S, J. R. Hipp, C. J. Young, 2009, Efficient and accurate calculation of ray theory seismic travel time through variable resolution 3D earth models, *Seismol. Res. Lett*. 80: 989–999.

Begnaud, M. L. (2005). Using a dedicated location database to enhance the gathering of ground truth information, Los Alamos National Laboratory document LA-UR-04-5992, 22 pp.

Bondár, I., S. C. Myers, E. R. Engdahl, and E. A. Bergman (2004). Epicentre accuracy based on seismic network criteria, *Geophys. J. Int.* 156: 483–496.

Crotwell, H.P., T.J. Owens, and J. Ritsema (1999). The TauP toolkit: flexible seismic travel-time and ray-path utilities, *Seism. Res. Lett*. 70: 154–160.

Kennett, B.L.N., E.R. Engdahl, R. Buland (1995). Constraints on seismic velocities in the Earth from taveltimes, *Geophys. J. Int*. 122: 108–124.

Laske, G. and T.G. Masters (1997), A global digital map of sediment thickness, *EOS Trans*. AGU, 78, F483.

Laske, G., T. G. Masters and C. Reif, CRUST 2.0: A New Global Crustal Model at 2x2 Degrees, http://igppweb.ucsd.edu/~gabi/crust2.html.

Li, S., and W. D. Mooney (1998). Crustal structure of China from deep seismic sounding profiles, in *Proceedings of the 7th international symposium on Deep seismic profiling of the continents,* Asilomar, CA, United States, *Tectonophysics* 288: 105–113.

Myers, S. C., M. L. Begnaud, S. Ballard, M. E. Pasyanos, W. S. Phillips, A. L. Ramirez, M. S. Antolik, K. D. Hutchenson, G. S. Wagner, J. J. Dwyer, C. A. Rowe, and D. R. Russell (2010). A crust and upper mantle model of Eurasia and North Africa for Pn travel time calculation, *Bull. Seismol. Soc. Am*. 100: 2, 640–656.

Simmons, N. A., S. C. Myers and A. Ramirez (2009). Multi-Resolution Seismic Tomography Based on a Recursive Tessellation Hierarchy, in *Proceedings of the 2009 Monitoring Research Review: Ground-Based Nuclear Explosion Monitoring Technologies*, LA-UR-09-05276, Vol. 1, pp. 211–220.

Um, J. and C. H. Thurber (1987). A fast algorithm for two-point seismic ray tracing, *Bull. Seismol. Soc. Am*. 77: 972–986.

Zhao, D. and J. Lei (2004), Seismic ray path variations in a 3D global velocity model, *Phys. Earth Planet In*. 141: 153–166.

Wang, Z., and F. A. Dahlen (1995), Spherical-Spline Parameterization of Three-Dimensional Earth Models, *Geophys. Res. Lett*. 22: (22), 3099–3102.